ACS Sustainable Chemistry & Engineering

Research Article

Cite This: ACS Sustainable Chem. Eng. 2019, 7, 2852−2859

pubs.acs.org/journal/ascecg

Novel Dual-Action Plant Fertilizer and Urease Inhibitor: Urea·Catechol Cocrystal. Characterization and Environmental Reactivity

Lucia Casali,[†] Luca Mazzei,[‡] Oleksii Shemchuk,[†] Lohit Sharma,[§] Kenneth Honer,[§] Fabrizia Grepioni,*[,†] Stefano Ciurli,*[,‡] Dario Braga,[†] and Jonas Baltrusaitis*[,§]

[†]Molecular Crystal Engineering Laboratory, Department of Chemistry "Giacomo Ciamician", University of Bologna, Via F. Selmi, 2, 40126 Bologna, Italy

[‡]Laboratory of Bioinorganic Chemistry, Department of Pharmacy and Biotechnology, University of Bologna, Viale Giuseppe Fanin 40, 40127 Bologna, Italy

[§]Department of Chemical and Biomolecular Engineering, Lehigh University, 111 Research Drive, Bethlehem, Pennsylvania 18015, United States

Supporting Information

ABSTRACT: The mechanochemical reaction of urea and catechol affords the quantitative formation of a 1:1 urea·catechol (URCAT) cocrystal that can act simultaneously as a urease inhibitor and as a soil fertilizer. The novel compound has been characterized using solid-state methods, and its environmental activity has been assessed using the inhibition of *Canavalia ensiformis* urease and water vapor sorption experiments at room temperature. The urea molecules within the cocrystal were organized in hydrogen-bonded dimers bridged by two catechol molecules, with the OH groups interacting via hydrogen bonds with the urea carbonyl groups. The inhibition of jack bean urease enzyme by URCAT led to the complete loss of urease activity after a 20 min incubation period. A large difference of water vapor adsorption was observed between urea and URCAT, with the latter adsorbing 3.5 times less water than urea. Our results suggested that cocrystal engineering strategies can be successfully applied to tackle sustainability problems at the food−energy−water nexus.

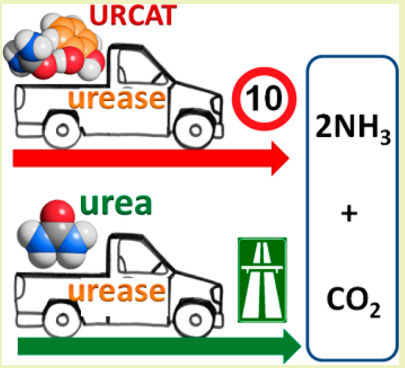

KEYWORDS: *Nitrogen, Urea, Cocrystal, Environment, Nutrients*

INTRODUCTION

Urea is a major nitrogen (N)-containing soil fertilizer, synthesized from ammonia (NH_3) and carbon dioxide (CO_2), with an annual production projected to reach 226 million tons in 2021.[1] Once deposited in soil, urea quickly hydrolyzes in a moist environment to yield NH_4^+ and HCO_3^-.[2] This reaction causes a number of agronomic,[3] environmental,[4−6] and economic[7−9] problems[10] and affects the global N cycle.[11−13] In particular, too rapid of an increase in soil pH upon urea hydrolysis, catalyzed by urease activity,[14] causes the loss of urea nitrogen as gaseous NH_3. Ammonia is toxic to plants[15] and contributes to the production of fine inorganic particulate matter ($PM_{2.5}$),[16] a well-documented factor for premature population mortality,[17] as ammonium−sulfate−nitrate salts.[18] Furthermore, ammonia nitrification produces additional N loss due to nitrate leaching or denitrification, the latter causing tropospheric pollution by NO, NO_2, and especially N_2O, a greenhouse gas with 300 times the heat-trapping capacity of CO_2.[9,13] Exogenous inorganic and organic molecules are often introduced into soil with urea to inhibit urease activity, thus affecting urea chemistry.[19] Reversible inhibitors that target the Ni(II) ions in the active urease site can be utilized, such as phosphate, diamidophosphate, thiols, sulfite, and fluoride as well as hydroxamic, citric, and boric acids, whereas Michael-type reagents such as catechols or quinones irreversibly target enzyme cysteine thiols essential for catalysis.[14,20−22] A widely used urease inhibitor is the organophosphorus compound *N*-(*n*-butyl)thiophosphoric triamide (NBPT), whose mechanism of action has been recently elucidated.[23] Considering that some negative effects of NBPT on living cells of plants[24,25] and microorganisms[26] have been reported, conceptually new methods to mitigate urea reactivity need to be developed. Within this framework, an approach based on acidic polymers was shown to be effective.[27] Recent attempts to improve urea stability[28−31] in soil have exploited its excellent and well-established propensity to form molecular and ionic cocrystals.[32−35] In particular, two types of urea cocrystals have been utilized to stabilize its reactivity toward hydrolysis and decrease concurrent emissions of ammonia.

Received: December 1, 2018
Revised: December 20, 2018
Published: December 24, 2018

DOI: 10.1021/acssuschemeng.8b06293
ACS Sustainable Chem. Eng. 2019, 7, 2852−2859

First, urea physicochemical stabilization via encapsulation with ionic metal salts or the corresponding acids was utilized. Some field measurement evidence reveals that urea coordination compounds can reduce N losses from soils. For example, agricultural field tests with NH_4Cl or $ZnSO_4$ have been shown to reduce NH_3 losses from soil and improve overall nitrogen uptake efficiency when compacted with urea.[36] The inhibition of urea reactivity by organic or inorganic acids, such as phosphoric acid, was shown to decrease NH_3 emissions up to 50% from soil fertilized with urea phosphate ionic cocrystal.[37] Von Rheinbaben[38] and Fenn et al.[39] showed a significant decrease in NH_3 emissions for applied or reactively formed urea·$Mg(Ca)SO_4$ (or presumably urea adducts with $CaCl_2$ and $Ca(NO_3)_2$ formed in situ in soil), but the reaction mechanisms put forth were inconclusive, as other authors showed that sulfate salts were not effective NH_3 emission regulators.[40] Very recently, green mechanochemical methods were applied to synthesize urea ionic cocrystals, including 4urea·$CaSO_4$, directly from salts[30] and using reactive mechanochemistry[31] with urea inorganic acid cocrystals.

Second, urea cocrystals with urease-inhibiting metals or organic compounds have been utilized. Recently, it has been shown that metal ions acting as urease inhibitors, such as Zn^{2+}, can be associated within the same ionic cocrystal with plant nutrients, such as K^+, and with urea.[28] The cocrystal urea·$ZnCl_2$·KCl has been shown to effectively inhibit urease activity in a concentration-dependent manner. An old study on the inhibition of urease activity in soils showed that diphenols and quinones are particularly effective.[14] Recently, the kinetics of urease inhibition by benzoquinone and the structure of the corresponding urease-inhibitor complex have been elucidated.[41] Catechol (1,2-dihydroxybenzene) is another type of polyphenol that has been known for several decades to inhibit soil urease,[14] but only recently has its mode of action been elucidated through a combined kinetic and structural study.[42]

In this Article, we report on the preparation, structural characterization, and evaluation of the environmental activity of a novel double-action material based on the association of urea with catechol. The objective is to provide, simultaneously, a potent urease inhibitor, catechol, together with a fundamental high-N-content fertilizer, such as urea.

EXPERIMENTAL SECTION

Reagents and Solutions. All reagents were purchased from Sigma-Aldrich or Alfa Aesar and used without further purification.

Solution Synthesis. Equimolar quantities of the starting materials (0.58 mmol) were dissolved in water or ethanol and left to evaporate at room temperature.

Solid-State Synthesis. The cocrystal was obtained by ball-milling urea (1 mmol) with catechol (1 mmol) in an agate jar for 60 min under dry conditions or with the addition of a drop of water.

Single-Crystal Growth. Single crystals suitable for X-ray diffraction were grown from an ethanol solution of the reagents in 1:1 stoichiometric ratio.

Slurry Experiments. Slurry experiments were performed in water at room temperature for 1 week to check for the possible formation of different solid forms. In all cases, the urea·catechol cocrystal was recovered.

Differential Scanning Calorimetry. Differential scanning calorimetry (DSC) traces were recorded using a PerkinElmer Diamond apparatus. The samples (1−3 mg range) were placed in open Al pans. All measurements were conducted in the range 40−150/160/170 °C (for urea, catechol, and URCAT) at a heating rate of 5 °C min^{-1}. DSC traces are reported in the Supporting Information (SI).

Thermogravimetric Analysis. Thermogravimetric analysis (TGA) measurements were performed with a PerkinElmer TGA7 in the temperature range 30−300 °C, under N_2 gas flow at a heating rate of 5 °C min^{-1}.

Single-Crystal X-ray Diffraction. Single-crystal data were collected at room temperature with an Oxford X'Calibur S CCD diffractometer equipped with a graphite monochromator (Mo−Kα radiation, λ = 0.71073 Å). Data collection and refinement details are listed in Table S1. The structure were solved with SHELXT-2014[43] and refined on full-matrix F^2 by means of SHELXL-2014[43] implemented in the Olex2 software.[44] All non-hydrogen atoms were refined anisotropically. Hydrogen atoms bound to nitrogen or oxygen atoms were either located from the Fourier map or added in calculated positions; H_{CH} atoms were added in calculated position. All H atoms were refined riding on the corresponding C/N/O atoms. The software Mercury 3.10[45] was used to simulate powder patterns based on single-crystal data. The program Schakal was used for graphical representations.[46] CCDC 1880413 contains the supplementary crystallographic data for this paper. These data are provided free of charge by The Cambridge Crystallographic Data Centre (CCDC).

X-ray Diffraction from Powder. X-ray diffraction patterns were collected on a PANalytical X'Pert Pro automated diffractometer equipped with an X'celerator detector in Bragg−Brentano geometry using Cu−Kα radiation (λ = 1.5418 Å) without monochromator in the 3−50° 2θ range (step size 0.033°; time/step: 20 s; Soller slit 0.04 rad, antiscatter slit: 1/2, divergence slit: 1/4; 40 mA*40 kV).

Urease Inhibition Experiments. The inhibition of urease by URCAT was characterized at room temperature through preincubation experiments carried out by following a spectrophotometric assay in which cresol red was exploited as a colorimetric probe to monitor the overtime change in absorbance at 573 nm due to the increase in pH caused by urease activity.[42] A 100 μL solution of 30 nM urease from *Canavalia ensiformis* (jack bean) urease (JBU) dissolved in 50 mM HEPES buffer at pH 7.5 was diluted to 0.3 nM in 9.86 mL of 2 mM HEPES buffer at pH 7.50, also containing 2 mM EDTA and 30 mg L^{-1} cresol red (CR solution). A 40 μL solution of 10 mM URCAT or catechol, dissolved in the same buffer, was added, taking the time when the enzyme solution and URCAT (or catechol) were mixed as zero time of incubation. After appropriate periods of time, 1 mL aliquots were withdrawn from the incubation solution, an 8 M solution of urea was added to a final concentration of 100 mM, and the change in absorbance over time was followed (λ = 573 nm). The activity was calculated by a linear fitting of the straight portion in the absorbance versus time curve and normalized to the activity measured at time zero of incubation.

Dynamic Vapor Sorption Experiments. The DVS Intrinsic dynamic vapor sorption (DVS) apparatus (Surface Measurement Systems, USA), equipped with an SMS ultrabalance having a mass resolution of ±0.1 μg, was used to obtain ramping and equilibrium water vapor sorption isotherms. Approximately 5 mg of powder samples was placed in the apparatus using aluminum pans and initially dried over 600 min with a stream of dry nitrogen to establish a dry mass at 25 °C. The dry mass was calculated after the end of the first drying stage (0% RH). The sorption cycle experiments were performed from 0% relative humidity (RH) to 95% RH in a step of 5% RH in a preprogrammed sequence before decreasing to 0% RH in a reverse order. The instrument maintained a constant target RH until the moisture content change per minute (dm/dt) was <0.002% per minute over a 10 min period.

The GAB analysis (Guggenheim−Anderson−DeBoer) isotherm,[47] with constants C_G and K, was converted to a second-order polynomial, giving a quadratic equation. The curve fitting parameters was evaluated using mean-square error and mean relative percentage deviation.

The GAB model is given in eq 1

$$\frac{W}{W_m} = \frac{C_G{*}K{*}a_w}{(1 - K{*}a_w)[1 - K{*}a_w + C_G{*}K{*}a_w]} \quad (1)$$

DOI: 10.1021/acssuschemeng.8b06293
ACS Sustainable Chem. Eng. 2019, 7, 2852−2859

where W is water content on a dry-weight basis, W_m is one molecule water per active sorption site, a_w is the water activity, C_G is the GAB sorption constant, and K is a parameter in the GAB equation. Most isotherm models in the literature, including BET and GAB, assume surface sorption only. For instance, BET and GAB describe monolayer water adsorption, followed by multilayer water. These models are not able to accurately describe bulk, solution, or absorbed water. Therefore, a GAB fitting procedure was applied here only to compare urea and URCAT qualitative differences upon water vapor adsorption.

RESULTS AND DISCUSSION

Urea·Catechol Cocrystal Structure. The URCAT cocrystal of urea and catechol was prepared by milling of the two reactants in a 1:1 stoichiometric ratio. (See the Experimental Section.) Single crystals suitable for X-ray diffraction were grown from an ethanol solution of the reagents. The structural identity between the product of the solid-state synthesis and the product of the recrystallization via seeding was verified by comparing the X-ray powder diffraction (XRPD) pattern, calculated on the basis of the single-crystal structure, and the experimental pattern measured for the crystalline powder. (See Figure 1.)

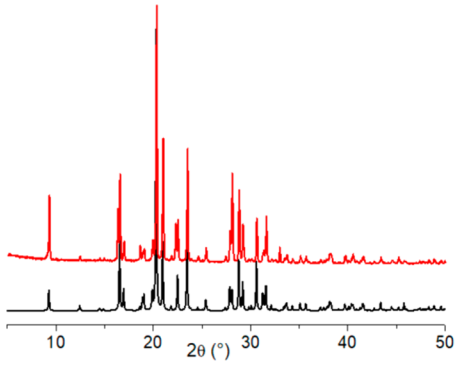

Figure 1. Comparison between the experimental patter (black line) measured of the product of the solid-state synthesis and the pattern (red line) calculated on the basis of the single-crystal structure.

Figure 2 shows the main packing feature of crystalline URCAT: Urea is organized in hydrogen-bonded dimers,

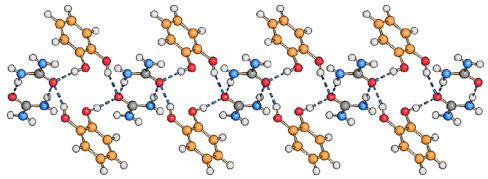

Figure 2. Main packing feature in crystalline URCAT: Urea is organized in hydrogen-bonded dimers, which are bridged by catechol molecules, thus resulting in the formation of infinite ribbons. C (urea) atoms in gray, C (catechol) atoms in orange.

similar to what is observed in its pure crystal,[48] as shown in Figure 3a; all dimers are bridged by two catechol molecules, with the OH groups interacting via hydrogen bonds with the urea carbonyl groups [$O_{OH}\cdots O_{CO}$ 2.717(3) Å].

This results in the formation of infinite ribbons extending along the crystallographic a axis. When comparing the crystal packing of the cocrystal with that of catechol[48] shown in Figure 3b, it can be seen that in pure catechol all molecules form

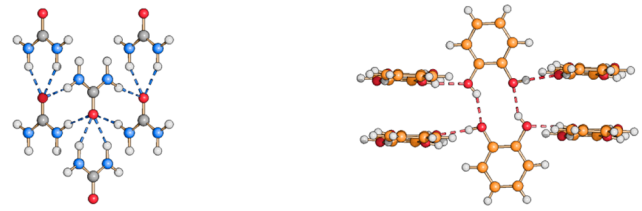

(a) (b)

Figure 3. Hydrogen-bonded dimers in crystalline urea (a) and catechol (b).

hydrogen-bonded dimers. In turn, each dimer interacts with four neighboring dimers arranged perpendicularly to the dimer plane. Therefore, the main difference arises from the fact that catechol in the cocrystal is hydrogen-bonded only to urea; a similar pattern is present in the known catechol·2DMSO solvate[49] (refcode EPAVUN, Figure 4): Here hydrogen-

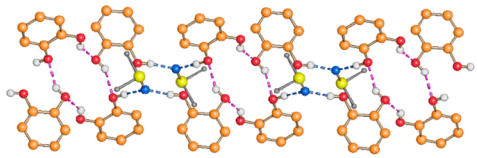

Figure 4. Hydrogen-bonded ribbon involving catechol and DMSO in the catechol·2DMSO solvate (EPAVUN). H_{CH} atoms are not shown for clarity; small gray spheres represent the methyl groups.

bonded tetramers can be identified and are formed by catechol molecules only, whereas the tetramers are bridged by the DMSO S=O groups, resulting in the formation of rings similar to those observed in crystalline URCAT (Figure 2); all units are arranged in infinite ribbons extending along the crystallographic c axis.

Thermal Stability of the Cocrystal. DSC measurements were performed using the urea·catechol cocrystal and the starting materials, that is, urea and catechol, in the 40−150 °C range. No thermal events are present for the cocrystal before melting, which occurs at 76.4 °C (peak temperature). The cocrystal thus melts at a temperature that is definitely lower than those of its components, as can be seen from Figure 5. TGA measurements also show that on heating the cocrystal is stable up to ca. 80 °C; that is, melting is almost immediately followed by decomposition.

Urease Inhibition Experiments. The inhibition of *Canavalia ensiformis* JBU by URCAT was studied by preincubating the enzyme with 40 μM inhibitor for increasing periods of time, as previously described,[41,42] and the residual activity was monitored using UV−vis spectrophotometry. The inhibition of the enzyme by 40 μM catechol was also determined and used as a control, and it is in complete agreement with previously published data.[42] The data in Figure 6 reporting the residual activity of urease as a function of preincubation time show a time-dependent inactivation process. In particular, a short initial lag phase is followed by an acceleration of the inactivation course that yields a 50% inactivation in ca. 5 min, leading to the eventual complete loss of urease activity in a 20 min period. The inactivation efficiency of URCAT on urease is largely comparable to that of catechol under the experimental conditions used, demonstrat-

DOI: 10.1021/acssuschemeng.8b06293
ACS Sustainable Chem. Eng. 2019, 7, 2852−2859

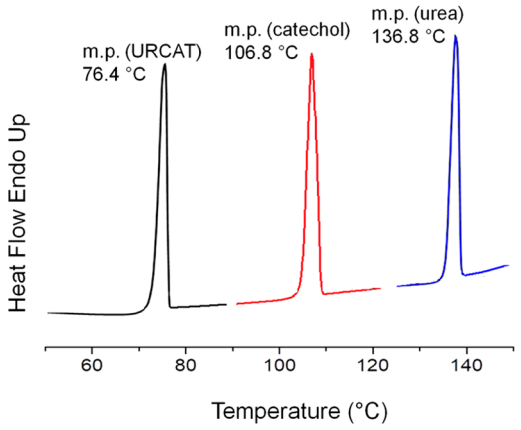

Figure 5. Comparison of the DSC traces for (from left to right) URCAT, catechol, and urea.

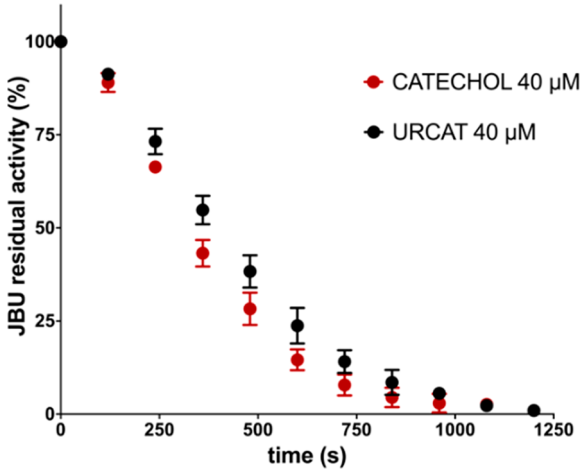

Figure 6. Residual JBU activity as a function of preincubation time of the enzyme in the presence of 40 μM URCAT (black dots) or 40 μM catechol (red dots). Data were measured as triplicates; mean and standard deviation (as bars) are reported.

ing that URCAT is a catechol·urea coformulate efficient in controlling the urease activity in vitro.

Dynamic Vapor Sorption Analysis. The amount of adsorbed water as well as urea and URCAT response to changes in RH were investigated using constant temperature adsorption/desorption experiments by varying water as RH. Results are shown in Figure 7. In particular, URCAT, when normalized per unit of surface area, m^2, adsorbs ~3.5 less water than urea at high RH. The RH here is defined as where P_o is the saturated vapor pressure of water at 298 K and 1 atm, and P is the actual water pressure at the same temperature and pressure, for example

$$\mathrm{RH} = \frac{P}{P_o} \times 100\ (\%) \tag{2}$$

Additionally, both urea and URCAT DVS data exhibited hysteresis between the adsorption and desorption branches, albeit of different shapes. During the hydration of urea, water uptake remained negligible until deliquescence phase transition at 74% RH, indicating sharp size increase and liquid layer formation on urea. Subsequently, with further increases in RH, the aqueous droplet underwent continuous hygroscopic growth. During the dehydration process, the representative

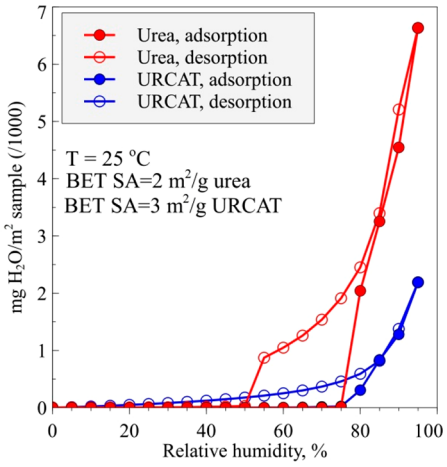

Figure 7. Adsorption/desorption branches of RH on urea and URCAT.

urea particle showed a two-stage phase transition. The liquid droplet decreased gradually in size with decreasing RH and became supersaturated with respect to urea below RH of 74%. With further decrease in RH, effloresced particle was formed at RH of 50%. Notably, URCAT lacks a distinct efflorescence point, as exhibited by a continuous hysteresis down to low (<20% RH) values of a desorption branch. The direct absence of an observable efflorescence point after deliquescence is reached suggests that some water remains bound in a structural form (H bond or monolayer), especially at low RH. Furthermore, water, still bound at intermediate RH (70 to 30%), can be regarded as the continuous transition of the bound-to-free water with the vaporization enthalpy slightly higher than that for pure water.[50] It potentially indicates that strong hydrogen bonds were formed with URCAT hydrophilic and polar groups.

The water sorption (and retention) of URCAT was further elucidated using the GAB analysis isotherm,[47,51−53] as shown in Figure 8. The GAB model represents a refined extension of the BET theory postulating that the state of the sorbate molecules in the second and higher layers is equal but different from that in the liquid-like state.[54] The fit parameters W_m (the monolayer moisture content), C_G, and K (constants related to the energies of interaction between the first and further

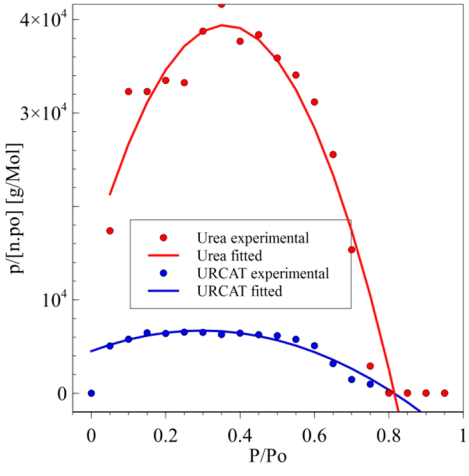

Figure 8. Resulting fits to the GAB model of urea and URCAT.

DOI: 10.1021/acssuschemeng.8b06293
ACS Sustainable Chem. Eng. 2019, 7, 2852−2859

molecules, for example, monolayer and multilayer regions at the individual sorption sites) are related to the sorption enthalpies.

Accordingly, URCAT exhibited greater monolayer capacity (mol/g) than urea, as shown in Table 1. Furthermore, the

Table 1. Calculated RH Absorption Parameters Obtained Using GAB Model

sample	W_m, monolayer capacity (mol/g)	sorption constant K	sorption constant C_G
urea	5.73×10^{-6}	1.221	9.931
URCAT	3.59×10^{-5}	1.264	4.850

sorption constant C_G, describing a monolayer formation propensity, is greater for urea than for URCAT, whereas the multilayer region constant K is very similar for both samples. The higher monolayer capacity in URCAT can be related to its ability to retain water even at low humidity, as shown in Figure 7. Urea, on the contrary, shows stronger binding affinity toward monolayer water, as C_G can be directly related to the difference between the monolayer and multilayer molar sorption enthalpies.[55,56]

Solubility Test. The solubility of urea at room temperature ranges from 1 to 1.2 g mL^{-1}, Therefore, a control experiment was conducted in which 1 g of urea was added to a vial and dissolved in 1 mL of bidistilled water. In a second vial, an amount of URCAT (2.8 g) containing 1 g of urea and 1 mL of bidistilled water was then added: The dissolution was not complete after 5 min, as can be seen in Figure 9.

Figure 9. Solubility test for URCAT in bidistilled water.

The undissolved solid was filtered and weighed, resulting in ca. 500 mg of powder material, which corresponds to a ca. 15% reduction of the solubility of urea in URCAT with respect to pure urea. The undissolved powder was analyzed via X-ray powder diffraction and found to be URCAT (Figure 10).

Stability Tests. URCAT (2.8 g) and a physical mixture of urea (1 g) and catechol (1.8 g) were placed in two separate watch glasses inside a chamber at controlled humidity (82% RH) (see Figure 11, top). Degradation of catechol, visually observed after ca. 5 h as a color change from white to pinkish-brown (see Figure 11, bottom left), was confirmed via X-ray powder diffraction (see Figure 12); the URCAT cocrystal, on the contrary, did not show any modification after 5 h, suggesting that the stability of catechol is markedly improved in URCAT with respect to pure catechol.

CONCLUSIONS AND SUSTAINABILITY IMPACT

URCAT has successfully been synthesized by milling of the components. The resulting compound has been investigated

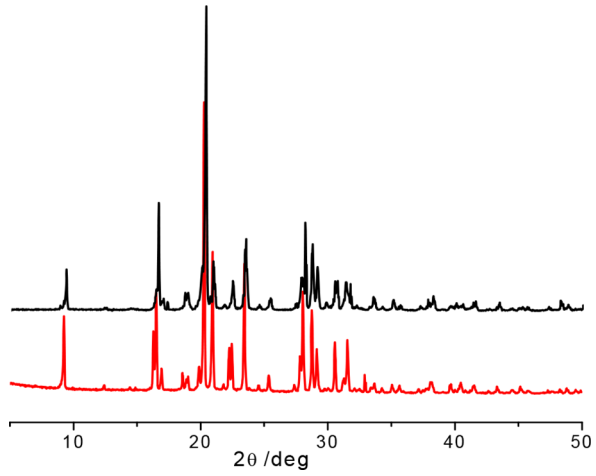

Figure 10. Experimental X-ray powder patterns for URCAT measured before the solubility test (red line) and on the residual powder after the solubility test (black line).

Figure 11. Visual comparison of the physical mixture of urea and catechol (left) and the URCAT cocrystal (right) at t = 0 (top) and after 5 h at 82% RH (bottom).

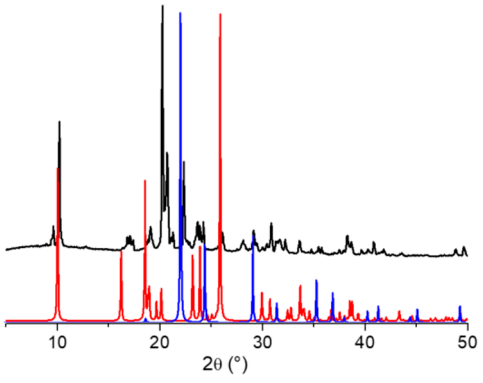

Figure 12. Comparison of the XRPD pattern measured on the physical mixture after 5 h of exposition to 82% RH (black line) and the calculated patterns of the pure components (blue line for urea, red line for catechol).

thoroughly with a combination of solid-state and biotechnological methods. Single crystals of URCAT have been grown from solution and fully structurally characterized. The urea molecules within the cocrystal are organized in hydrogen-bonded dimers bridged by two catechol molecules, with the OH groups interacting via hydrogen bonds with the urea

DOI: 10.1021/acssuschemeng.8b06293
ACS Sustainable Chem. Eng. 2019, 7, 2852−2859

carbonyl groups. The cocrystal exhibits a melting temperature of 76.4 °C, lower than that of pure reactants. The inhibition of JBU enzyme by URCAT leads to the complete loss of urease activity after a 20 min incubation period. These data are comparable to those of catechol itself, demonstrating that URCAT is a catechol−urea coformulate efficient in controlling urease activity in vitro. The stability of URCAT as compared with urea in the presence of H_2O vapor was inferred using DVS experiments. A large difference of water vapor adsorption was observed between urea and URCAT, with the latter adsorbing 3.5 times less water than urea. A higher propensity of URCAT to retain adsorbed water at low RH as compared with urea was also observed.

In conclusion, whereas the inhibition of urease activity with the previously investigated urea·$ZnCl_2$·KCl cocrystal was achieved via inorganic salt complexation,[28] the cocrystallization of urea and catechol affords an organic-only material that can act both as soil fertilizer and efficacious urease inhibitor. Our results lend further support to the idea that cocrystal engineering strategies[57] can be successfully applied to tackle agricultural, food production, and environmental issues. In particular, the food, energy, and water systems are delicately linked in conventional agricultural production, especially with respect to fertilizer systems. As the world's population and the corresponding food production continue to grow, meeting the fertilizer demands for crops will become more difficult and add increasing pressure on our water and energy systems. This is partially due to the nitrogen losses associated with the little environmental stability of urea under humid conditions. Our results show that URCAT can not only serve as an inhibitor to minimize urea nitrogen losses but also possess improved environmental stability. Utilizing such urea cocrystals has the ability to decrease a significant portion of fertilizer demand while potentially enhancing this food−energy−water system sustainability. If effective in the field, it may help lower ammonia emissions and increase nitrogen use efficiency by using less product (smaller environmental footprint) to maintain crop yields for a growing population. Finally, if effective in the field, it may help lower the amount of nitrate leaching. This would allow plants more of an opportunity to uptake nitrate before the nitrate is leached beneath the rooting zone.

■ ASSOCIATED CONTENT

Supporting Information

The Supporting Information is available free of charge on the ACS Publications website at DOI: 10.1021/acssuschemeng.8b06293.

TGA, DSC, crystal data, and details of measurement for URCAT (PDF)

■ AUTHOR INFORMATION

Corresponding Authors

*J.B.: E-mail: job314@lehigh.edu.
*F.G.: E-mail: fabrizia.grepioni@unibo.it.
*S.C.: E-mail: stefano.ciurli@unibo.it.

ORCID

Oleksii Shemchuk: 0000-0003-3003-3922
Fabrizia Grepioni: 0000-0003-3895-0979
Stefano Ciurli: 0000-0001-9557-926X
Jonas Baltrusaitis: 0000-0001-5634-955X

Notes

The authors declare no competing financial interest.

■ ACKNOWLEDGMENTS

This material is based on the work of K.H. and J.B. supported by the National Science Foundation under Grant Number CHE-1710120 and on the work of D.B., F.G., L.M., and S.C. supported by the University of Bologna (RFO scheme).

■ REFERENCES

(1) Agriculture and Production & International Trade Services. Fertilizer Outlook 2017−2021. In *International Fertilizer Association (IFA) Annual Conference, Marrakech (Marocco), 22−24 May 2017*; International Fertilizer Association, 2017.

(2) Zhu, X.; Burger, M.; Doane, T. A.; Horwath, W. R. Ammonia Oxidation Pathways and Nitrifier Denitrification Are Significant Sources of N(2)O and NO under Low Oxygen Availability. *Proc. Natl. Acad. Sci. U. S. A.* **2013**, *110* (16), 6328−6333.

(3) Hewitt, C. N.; MacKenzie, A. R.; Di Carlo, P.; Di Marco, C. F.; Dorsey, J. R.; Evans, M.; Fowler, D.; Gallagher, M. W.; Hopkins, J. R.; Jones, C. E.; Langford, B.; Lee, J. D.; Lewis, A. C.; Lim, S. F.; McQuaid, J.; Misztal, P.; M?ller, S. J.; Monks, P. S.; Nemitz, E.; Oram, D. E.; Owen, S. M.; Phillips, G. J.; Pugh, T. A.; Pyle, J. A.; Reeves, C. E.; Ryder, J.; Siong, J.; Skiba, U.; Stewart, D. J. Nitrogen Management Is Essential to Prevent Tropical Oil Palm Plantations from Causing Ground-Level Ozone Pollution. *Proc. Natl. Acad. Sci. U. S. A.* **2009**, *106* (44), 18447−18451.

(4) Oikawa, P. Y.; Ge, C.; Wang, J.; Eberwein, J. R.; Liang, L. L.; Allsman, L. A.; Grantz, D. A.; Jenerette, G. D. Unusually High Soil Nitrogen Oxide Emissions Influence Air Quality in a High-Temperature Agricultural Region. *Nat. Commun.* **2015**, *6*, 8753.

(5) Diaz, R. J.; Rosenberg, R. Spreading Dead Zones and Consequences for Marine Ecosystems. *Science (Washington, DC, U. S.)* **2008**, *321* (5891), 926−929.

(6) Duce, R. A.; LaRoche, J.; Altieri, K.; Arrigo, K. R.; Baker, A. R.; Capone, D. G.; Cornell, S.; Dentener, F.; Galloway, J.; Ganeshram, R. S.; Geider, R. J.; Jickells, T.; Kuypers, M. M.; Langlois, R.; Liss, P. S.; Liu, S. M.; Middelburg, J. J.; Moore, C. M.; Nickovic, S.; Oschlies, A.; Pedersen, T.; Prospero, J.; Schlitzer, R.; Seitzinger, S.; Sorensen, L. L.; Uematsu, M.; Ulloa, O.; Voss, M.; Ward, B.; Zamora, L. Impacts of Atmospheric Anthropogenic Nitrogen on the Open Ocean. *Science (Washington, DC, U. S.)* **2008**, *320* (5878), 893−897.

(7) Galloway, J. N.; Cowling, E. B. Reactive Nitrogen and the World: 200 Years of Change. *Ambio* **2002**, *31* (2), 64−71.

(8) Galloway, J. N.; Aber, J. D.; Erisman, J. W.; Seitzinger, S. P.; Howarth, R. W.; Cowling, E. B.; Cosby, B. J. The Nitrogen Cascade. *BioScience* **2003**, *53* (4), 341−356.

(9) Galloway, J. N.; Dentener, F. J.; Capone, D. G.; Boyer, E. W.; Howarth, R. W.; Seitzinger, S. P.; Asner, G. P.; Cleveland, C. C.; Green, P. A.; Holland, E. A.; Karl, D. M.; Michaels, A. F.; Porter, J. H.; Townsend, A. R.; Vörösmarty, C. J. Nitrogen Cycles: Past, Present, and Future. *Biogeochemistry* **2004**, *70* (2), 153−226.

(10) Kiss, S.; Simihaian, M. *Improving Efficiency of Urea Fertilizers by Inhibition of Soil Urease Activity*; Springer: The Netherlands, 2002.

(11) Zhang, X.; Davidson, E. A.; Mauzerall, D. L.; Searchinger, T. D.; Dumas, P.; Shen, Y. Managing Nitrogen for Sustainable Development. *Nature* **2015**, *528*, 51−59.

(12) Rockström, J.; Steffen, W.; Noone, K.; Persson, Å.; Chapin, F. S., III; Lambin, E. F.; Lenton, T. M.; Scheffer, M.; Folke, C.; Schellnhuber, H. J.; Nykvist, B.; de Wit, C. A.; Hughes, T.; van der Leeuw, S.; Rodhe, H.; Sörlin, S.; Snyder, P. K.; Costanza, R.; Svedin, U.; Falkenmark, M.; Karlberg, L.; Corell, R. W.; Fabry, V. J.; Hansen, J.; Walker, B.; Liverman, D.; Richardson, K.; Crutzen, P.; Foley, J. A. A Safe Operating Space for Humanity. *Nature* **2009**, *461*, 472−475.

(13) Coskun, D.; Britto, D. T.; Shi, W.; Kronzucker, H. J. Nitrogen Transformations in Modern Agriculture and the Role of Biological Nitrification Inhibition. *Nat. Plants* **2017**, *3*, 17074.

DOI: 10.1021/acssuschemeng.8b06293
ACS Sustainable Chem. Eng. 2019, 7, 2852−2859

(14) Bremner, J. M.; Douglas, L. A. Inhibition of Urease Activity in Soils. *Soil Biol. Biochem.* **1971**, *3* (4), 297−307.
(15) Krupa, S. V. Effects of Atmospheric Ammonia (NH3) on Terrestrial Vegetation: A Review. *Environ. Pollut.* **2003**, *124* (2), 179−221.
(16) Hand, J. L.; Schichtel, B. A.; Pitchford, M.; Malm, W. C.; Frank, N. H. Seasonal Composition of Remote and Urban Fine Particulate Matter in the United States. *J. Geophys. Res. Atmos.* **2012**, *117*, D05209.
(17) Pope, C. A.; Ezzati, M.; Dockery, D. W. Fine-Particulate Air Pollution and Life Expectancy in the United States. *N. Engl. J. Med.* **2009**, *360* (4), 376−386.
(18) Paulot, F.; Jacob, D. J. Hidden Cost of U.S. Agricultural Exports: Particulate Matter from Ammonia Emissions. *Environ. Sci. Technol.* **2014**, *48* (2), 903−908.
(19) Kafarski, P.; Talma, M. Recent Advances in Design of New Urease Inhibitors: A Review. *J. Adv. Res.* **2018**, *13*, 101−112.
(20) Zambelli, B.; Musiani, F.; Benini, S.; Ciurli, S. Chemistry of Ni^{2+} in Urease: Sensing, Trafficking, and Catalysis. *Acc. Chem. Res.* **2011**, *44* (7), 520−530.
(21) Mazzei, L.; Musiani, F.; Ciurli, S. Chapter 5. Urease. In *The Biological Chemistry of Nickel*; The Royal Society of Chemistry, 2017; pp 60−97.
(22) Maroney, M. J.; Ciurli, S. Nonredox Nickel Enzymes. *Chem. Rev.* **2014**, *114* (8), 4206−4228.
(23) Mazzei, L.; Cianci, M.; Contaldo, U.; Musiani, F.; Ciurli, S. Urease Inhibition in the Presence of N-(n-Butyl)Thiophosphoric Triamide, a Suicide Substrate: Structure and Kinetics. *Biochemistry* **2017**, *56* (40), 5391−5404.
(24) Krogmeier, M. J.; McCarty, G. W.; Bremner, J. M. Potential Phytotoxicity Associated with the Use of Soil Urease Inhibitors. *Proc. Natl. Acad. Sci. U. S. A.* **1989**, *86* (4), 1110−1112.
(25) Zanin, L.; Tomasi, N.; Zamboni, A.; Varanini, Z.; Pinton, R. The Urease Inhibitor NBPT Negatively Affects DUR3-Mediated Uptake and Assimilation of Urea in Maize Roots. *Front. Plant Sci.* **2015**, *6*, 1007.
(26) Tarsia, C.; Danielli, A.; Florini, F.; Cinelli, P.; Ciurli, S.; Zambelli, B. Targeting *Helicobacter Pylori* Urease Activity and Maturation: In-Cell High-Throughput Approach for Drug Discovery. *Biochim. Biophys. Acta, Gen. Subj.* **2018**, *1862* (10), 2245−2253.
(27) Mazzei, L.; Broll, V.; Ciurli, S. An Evaluation of Maleic-Itaconic Copolymers as Urease Inhibitors. *Soil Sci. Soc. Am. J.* **2018**, *82*, 994−1003.
(28) Casali, L.; Mazzei, L.; Shemchuk, O.; Honer, K.; Grepioni, F.; Ciurli, S.; Braga, D.; Baltrusaitis, J. Smart Urea Ionic Co-Crystals with Enhanced Urease Inhibition Activity for Improved Nitrogen Cycle Management. *Chem. Commun.* **2018**, *54* (55), 7637−7640.
(29) Sandhu, B.; Sinha, A. S.; Desper, J.; Aakeröy, C. B. Modulating the Physical Properties of Solid Forms of Urea Using Co-Crystallization Technology. *Chem. Commun.* **2018**, *54* (37), 4657−4660.
(30) Honer, K.; Kalfaoglu, E.; Pico, C.; McCann, J.; Baltrusaitis, J. Mechanosynthesis of Magnesium and Calcium Salt−Urea Ionic Cocrystal Fertilizer Materials for Improved Nitrogen Management. *ACS Sustainable Chem. Eng.* **2017**, *5* (10), 8546−8550.
(31) Honer, K.; Pico, C.; Baltrusaitis, J. Reactive Mechanosynthesis of Urea Ionic Cocrystal Fertilizer Materials from Abundant Low Solubility Magnesium- and Calcium-Containing Minerals. *ACS Sustainable Chem. Eng.* **2018**, *6* (4), 4680−4687.
(32) Theophanides, T.; Harvey, P. D. Structural and Spectroscopic Properties of Metal-Urea Complexes. *Coord. Chem. Rev.* **1987**, *76*, 237−264.
(33) Smith, G.; Baldry, K. E.; Byriel, K. A.; Kennard, C. H. L. Molecular Cocrystals of Carboxylic Acids. XXV The Utility of Urea in Structure Making with Carboxylic Acids and the Crystal Structures of a Set of Six Adducts with Aromatic Acids. *Aust. J. Chem.* **1997**, *50* (7), 727−736.
(34) Hargittai, M. H. I. Novel Inclusion Compounds with Urea/Thiourea/Selenourea Anion Host Lattices. In *Advances in Molecular Structure Research*; Jai Press: 1998; pp 151−225.
(35) Huang, L.; Tonelli, A. E. Inclusion Compounds as a Means To Fabricate Controlled Release Materials. In *Intelligent Materials for Controlled Release*; ACS Symposium Series *728*; American Chemical Society, 1999; pp 10−131.
(36) Purakayastha, T. J.; Katyal, J. C. Evaluation of Compacted Urea Fertilizers Prepared with Acid and Non-Acid Producing Chemical Additives in Three Soils Varying in PH and Cation Exchange Capacity; I. NH3 Volatilization. *Nutr. Cycling Agroecosyst.* **1998**, *51* (2), 107−115.
(37) Moawad, H.; Enany, M. H.; El-Din, S. M. S. B.; Mahmoud, S. A. Z.; Gamal, R. F. Transformations and Effects of Urea Derivatives in Soil. *Z. Pflanzenernaehr. Bodenkd.* **1984**, *147* (6), 785−792.
(38) Von Rheinbaben, W. Effect of Magnesium Sulphate Addition to Urea on Nitrogen Loss Due to Ammonia Volatilization. *Fert. Res.* **1987**, *11* (2), 149−159.
(39) Fenn, L. B.; Richards, J. Ammonia Loss from Surface Applied Urea-Acid Products. *Fert. Res.* **1986**, *9* (3), 265−275.
(40) Fenn, L. B.; Hossner, L. R. Ammonia Volatilization from Ammonium or Ammonium-Forming Nitrogen Fertilizers. *Adv. Soil Sci.* **1985**, *1*, 123−169.
(41) Mazzei, L.; Cianci, M.; Musiani, F.; Ciurli, S. Inactivation of Urease by 1,4-Benzoquinone: Chemistry at the Protein Surface. *Dalt. Trans.* **2016**, *45* (13), 5455−5459.
(42) Mazzei, L.; Cianci, M.; Musiani, F.; Lente, G.; Palombo, M.; Ciurli, S. Inactivation of Urease by Catechol: Kinetics and Structure. *J. Inorg. Biochem.* **2017**, *166*, 182−189.
(43) Sheldrick, G. M. SHELXT - Integrated Space-Group and Crystal-Structure Determination. *Acta Crystallogr., Sect. A: Found. Adv.* **2015**, *A71*, 3−8.
(44) Dolomanov, O. V.; Bourhis, L. J.; Gildea, R. J.; Howard, J. A. K.; Puschmann, H. OLEX2: A Complete Structure Solution, Refinement and Analysis Program. *J. Appl. Crystallogr.* **2009**, *42* (2), 339−341.
(45) Macrae, C. F.; Edgington, P. R.; McCabe, P.; Pidcock, E.; Shields, G. P.; Taylor, R.; Towler, M.; van de Streek, J. Mercury: Visualization and Analysis of Crystal Structures. *J. Appl. Crystallogr.* **2006**, *39* (3), 453−457.
(46) Keller, E. Neues von SCHAKAL. *Chem. Unserer Zeit* **1986**, *20* (6), 178−181.
(47) van den Berg, C. Development of B.E.T.-Like Models for Sorption of Water on Foods, Theory, and Relevance. In *Properties of Water in Foods in Relation to Quality and Stability*; Simatos, D., Multon, J. L., Eds.; Springer Netherlands: Dordrecht, The Netherlands, 1985; pp 119−131.
(48) Brown, C. J. The Crystal Structure of Catechol. *Acta Crystallogr.* **1966**, *21* (1), 170−174.
(49) Polyanskaya, T. M.; Khaldoyanidi, K. A.; Smolentsev, A. I. Supramolecular Architecture of Catechol and Its 2:1 Complex with Dimethylsulfoxide. *J. Struct. Chem.* **2010**, *51* (2), 327−334.
(50) Basu, S.; Shivhare, U. S.; Mujumdar, A. S. Models for Sorption Isotherms for Foods: A Review. *Drying Technol.* **2006**, *24* (8), 917−930.
(51) Guggenheim, E. A. *Applications of Statistical Mechanics*; Oxford University Press, 1966.
(52) Anderson, R. B. Modifications of the Brunauer, Emmett and Teller Equation. *J. Am. Chem. Soc.* **1946**, *68* (4), 686−691.
(53) Boer, J. H. *The Dynamical Character of Adsorption*; Clarendon Press: Oxford, U.K., 1953.
(54) Al-Muhtaseb, A. H.; McMinn, W. A. M.; Magee, T. R. A. Moisture Sorption Isotherm Characteristics of Food Products: A Review. *Food Bioprod. Process.* **2002**, *80* (2), 118−128.
(55) van den Berg, C.; Bruin, S. Water Activity and Its Estimation in Food Systems: Theoretical Aspects. In *Water Activity: Influences on Food Quality*; Rockland, L. B., Stewart, G., Eds.; Academic Press, 1981; pp 1−61.

DOI: 10.1021/acssuschemeng.8b06293
ACS Sustainable Chem. Eng. 2019, 7, 2852−2859

(56) Kapsalis, J. G. Moisture Sorption Hysteresis. In *Water Activity: Influences on Food Quality*; Rockland, L. B., Stewart, G., Eds.; Academic Press, 1981; pp 143−177.
(57) Braga, D.; Grepioni, F.; Shemchuk, O. Organic−inorganic Ionic Co-Crystals: A New Class of Multipurpose Compounds. *CrystEngComm* **2018**, *20* (16), 2212−2220.

DOI: 10.1021/acssuschemeng.8b06293
ACS Sustainable Chem. Eng. 2019, 7, 2852−2859